Graphite-enhanced PCMs in Gypsum Boards for Reduced Building Energy Requirements

Chanita MANO, Somchai MANEEWAN, Atthakorn THONGTHA *

Department of Physics, Faculty of Science, Naresuan University, Phitsanulok, 65000, Thailand

http://doi.org/10.5755/j02.ms.37137

Received 2 May 2024; accepted 9 September 2024

The objective of this study is to improve the thermal characteristics of gypsum ceiling boards intended for building envelope applications, focusing on enhancing energy efficiency by integrating graphite-infused phase change material (PCM). The investigation examines PCM incorporation with graphite powder (PCM_{GP}) at 10 % and 20 % mass ratios using differential scanning calorimetry (DSC) analysis. The results indicate that the melting points of PCM, $PCM_{GP}-10$ %, and $PCM_{GP}-20$ % are approximately 59.6 °C, 59.6 °C, and 59.8 °C, respectively. Notably, the PCM_{GP}-10 % composite displays a narrower melting temperature range, signifying superior thermal characteristics. The PCM_{GP}-10 % composite layer significantly reduces the average room temperature by up to 3.79 % compared to non-PCM gypsum ceiling boards, up to 2.11 % compared to PCM layers without infused graphite, and up to 1.41 % compared to the PCM_{GP}-20 % composite layer under controlled temperature conditions when applied to gypsum ceiling boards. The optimized PCM_{GP} composite enhances thermal performance and thermal energy storage efficiency, leading to significant electrical energy savings by reducing cooling requirements within the building envelope. The implications of this study are crucial for sustainable construction materials and energy conservation strategies. Incorporating PCM_{GP} composites in building envelopes has the potential to enhance energy efficiency and thermal comfort, thus supporting sustainable and energy-efficient construction practices.

Keywords: phase change material, construction materials, graphite powder, energy saving, thermal storage.

1. INTRODUCTION

Over the past decade, energy use in buildings has increased due to rapid urbanization, population growth, increased durations spent indoors, and elevated standards of comfort and quality for indoor living [1]. Building energy consumption now constitutes a substantial portion of the global energy use, emphasizing the need for significant energy savings through optimal building design [2]. In tropical climates with high temperatures and solar intensity, buildings struggle with heat buildup [3]. Most energy in these areas goes towards cooling indoor spaces with air conditioning, which is an active cooling method requiring external energy to operate [4]. Therefore, passive cooling methods have emerged as viable alternatives to traditional cooling systems in response to this challenge, relying on natural processes for heat transfer without external power input [5].

Latent heat storage (LHS), particularly using Phase Change Materials (PCMs), has become a prominent passive method, improving the thermal inertia of building envelopes [6]. This strategy aims to stabilize temperature fluctuations, thereby enhancing indoor comfort for inhabitants [7]. PCMs, engineered for LHS, encompass a wide array of organic and inorganic compounds capable of transitioning between phases within temperature ranges optimized for distinct uses [8]. This distinctive feature allows PCMs to efficiently absorb and store substantial amounts of heat when transitioning between different states, subsequently releasing this heat when conditions change [9].

Recently, PCMs have been widely applied in different building envelope components, such as walls [10], windows [11], floors [12], roofs [13], and ceilings [14], significantly reducing energy consumption and notably improving thermal comfort within these structures.

Paraffin, as an organic PCM, has been applied in building applications due to its dependability, affordability, and notable LHS capabilities, and recognized safety [15]. However, its comparatively low thermal conductivity hinders its application as a PCM, limiting its adaptability in various applications [16]. This challenge has prompted numerous approaches to address the limitation, as evidenced in the existing literature [17 – 22].

For instance, C.Yadav and R.R. Sahoo [17] investigated natural convection in nano-enhanced PCM within a cylindrical thermal energy storage (TES) system. They measured temperature variations for stearic acid PCM with Al_2O_3 nano-additives, finding that a 0.3 % mass fraction reduced charging time by up to 16.6 %. In a different approach, S. M. Borhani et al. [18] developed a dynamic heat transfer model to analyze a heat exchanger utilizing metal foam-infused PCM under various flow conditions. Their findings indicated a 93.6 % decrease in melting time and improved heat storage rates with the use of metal foam. In a study by H.G. Kim et al. [19], thermal storage in concrete was explored using PCM/SiC-based composite aggregate. The study evaluated properties through Differential Scanning Calorimetry (DSC), conductivity assessments, and temperature evaluations. The results showed a phase transition of the composite at 33 – 34 °C,

* Corresponding author. Tel.: +66 559 63550 ; fax: +66 559 63501.
E-mail: *atthakornt@nu.ac.th* (A. Thongtha)

leading to a rise in internal temperatures by 2 – 10 °C, resulting in a 3 °C decrease in room temperature and enhanced TES. Meanwhile, M. Falcone et al. [20] investigated RT35 paraffin PCM using thermal cycles. Utilizing electrical top heating as their method, the researchers emphasized the benefits of incorporating a copper metal foam with 95 % porosity into a PCM storage system. This enhanced thermal conductivity improved heat transfer, reduced PCM melting time (29.54 % melting time reduction), and maintained temperatures below 20 K compared to pure PCM under the same top heat flux. B.M. Suyitno et al. [21] enhanced PCM-paraffin's thermal conductivity using volcanic ash, creating composites with 10 wt.%, 30 wt.%, and 50 wt.% ash. The $paraffin_{50}/ash_{50}$ composite improved thermal conductivity from 0.214 to 19.598 W/m·K and had a discharge rate of 4.21 ℃/min, much higher than pure paraffin's 1.69 ℃/min. In another study, T. Oya et al. [22] developed innovative Phase Change Composites (PCC) featuring erythritol PCM and graphite/nickel particles, achieving significantly higher thermal conductivity, surpassing the original PCM by two orders. Testing revealed notable enhancements, particularly with 20 vol.% spherical graphite, reaching 4.72 W/m·K with 15 vol.% expanded graphite, which is 6.4 times higher than pure erythritol.

The primary objective of the research is to enhance the efficiency of TES systems using paraffin, which is a PCM. To achieve this, the study proposes integrating paraffin with Graphite powder (GP), a material known for its high thermal conductivity. The primary objective of the research is to enhance the efficiency of TES systems using paraffin, which is a PCM. To achieve this, the study proposes integrating paraffin with GP, a material known for its high thermal conductivity. The integration of paraffin with GP is expected to significantly improve the thermal performance of PCM. To explore this enhancement, the study undertakes a comparative analysis of the thermal properties of paraffin in its standalone form and when combined with GP in a composite structure. The research employs DSC as a sophisticated analytical tool to thoroughly assess and compare the thermal characteristics of these configurations. This approach allows for a detailed examination of the heat flow and phase changes in the materials, providing valuable insights into their thermal behavior and potential for improving TES efficiency.

The investigation also evaluates the thermal performance of these materials when incorporated into ceiling boards. This is crucial as the heat transmissibility into the building's roof structure significantly contributes to daily heat transfer into indoor spaces. These investigations show that, in addition to increasing the thermal conductivity of paraffin using PCM with GP, this study also employed a novel approach by combining PCM_{GP} with the building envelope on the ceiling to reduce the temperature inside the building. Moreover, this application was evaluated under the temperature conditions of a tropical climate, a scenario rarely explored in previous research.

2. MATERIALS AND METHODS

2.1. Analysis and encapsulation of phase change materials

Paraffin, an organic PCM, showcases an impressive latent heat capacity. Derived from petroleum, coal, or tar, this white or colorless soft solid consists of hydrocarbon molecules, mainly from the alkane series, typically containing between 18 and 30 carbon atoms [23]. Paraffin wax exhibits a unique ability to absorb, retain, and cyclically release substantial heat during its transition from solid to liquid states. This property makes it an efficient material for LHS applications, where heat is absorbed or released without a significant change in temperature [24].

The PCM was melted and combined with graphite powder at 10 % and 20 % mass ratios, as shown in Fig. 1. To display homogeneity and prevent any irregularities, the mixtures were continuously stirred until they solidified, forming composites, as shown in Fig. 2.

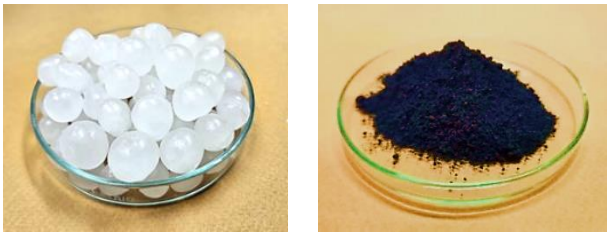

a b

Fig. 1. a – paraffin (PCM); b – graphite powder (GP)

The mass ratios of GP content in the PCM_{GP} mixtures were determined using Eq. 1.

$$\text{mass percentage of GP (\%)} = \frac{\text{mass of graphite powder (GP)}}{\text{mass of phase change material}} \times 100. \quad (1)$$

The mass ratios of 10 % and 20 % graphite powder have received special attention, as previous research [22] demonstrated that enhancing the thermal conductivity of PCMs with high thermal conductivity materials, particularly solid powders like graphite, can be achieved by mixing these powders in ratios of approximately 0 – 20 % by weight.

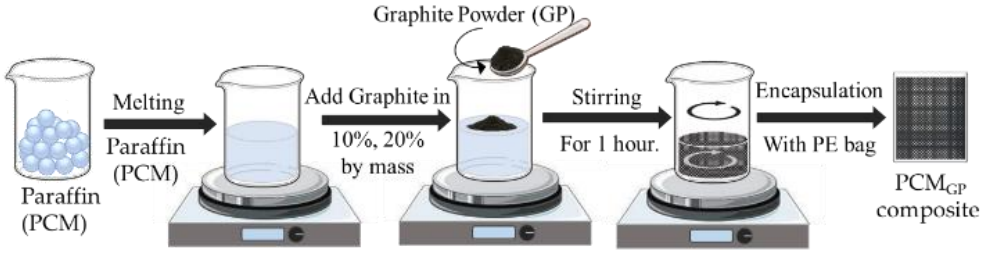

Fig. 2. The schematic of the PCM/graphite (PCM_{GP} – 10 % and PCM_{GP} – 20 – %) composites preparation

This approach increases the thermal conductivity of the PCM without significantly affecting the amount of PCM functioning as a latent heat storage.

Subsequently, the thermal process characteristics of PCM, $PCM_{GP}-10$ %, and $PCM_{GP}-20$ % were examined using DSC with a temperature range between 0 °C and 80 °C by applying a heating rate of 5 °C/min. The paraffin-type PCM was contained in polyethylene (PE) bags measuring 0.15 m × 0.15 m. Each PE bag contained approximately 50 g of PCM with a thickness of 0.001 m. These bags were arranged between two reflective plates, forming layers of PCM, $PCM_{GP}-10$ %, and $PCM_{GP}-20$ % with an area of 1.0 m × 1.0 m, as exhibited in Fig. 3.

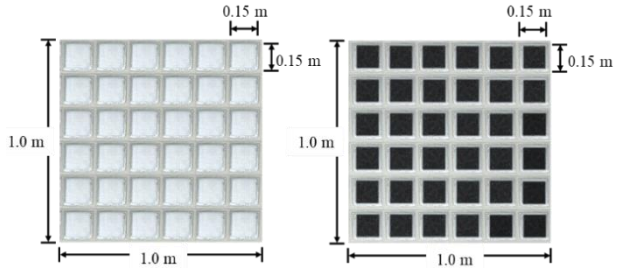

Fig. 3. The PCM and PCM_{GP} layout: a – the PCM layer samples; b – the PCM_{GP} layer samples for integrating into the ceiling board

2.2. Experimental set-up

The PCM, $PCM_{GP}-10$ %, and $PCM_{GP}-20$ % layers were integrated into the gypsum ceiling board. The dimensions of the testing design and the location of the thermal source installation are illustrated in Fig. 4 – Fig. 6, exhibiting a room with dimensions of 1.0 m × 1.0 m × 1.0 m. The walls and floor were constructed using 1 cm thick plywood sheets, with the interior wall insulated by 0.1 mm thick polyethylene sheets to prevent heat transfer. The ceiling component was constructed using a 0.5 cm thick gypsum board with dimensions of 1 m × 1 m, while the roof section was covered by a 0.5 cm thick metal sheet measuring 1 m × 1.3 m and inclined at a 40° angle from the horizontal. The model was thoroughly tested and controlled temperatures at 60 °C, 70 °C, and 80 °C, simulating heat exposure using a heat source of nine 500-watt halogen lamps. These lamps were positioned approximately 0.3 meters above the roof and controlled through a voltage dimmer.

Various temperatures were monitored using K-type thermocouples with an accuracy of approximately ± 0.5 °C at key locations in the experimental setup. These locations included above the metal roofing sheet (T_{AR}), outside surface temperature of the roof (T_{R1}), inside surface temperature of the roof (T_{R2}), attic space temperature (T_{AT}), PCM/PCM_{GP} layer temperature (T_{PCM}), upper ceiling surface temperature (T_{C1}), lower ceiling surface temperature (T_{C2}), interior room temperature (T_{Room}), and ambient temperature (T_{AB}), as exhibit in Fig. 4 – Fig. 6. Throughout the 300-minute experiment, temperature readings at each position were measured and recorded continuously in 1-minute intervals using a data logger. The ambient temperature was maintained at approximately 25 °C through the use of an air conditioner. This comprehensive monitoring aimed to investigate the thermal fluctuation under various conditions.

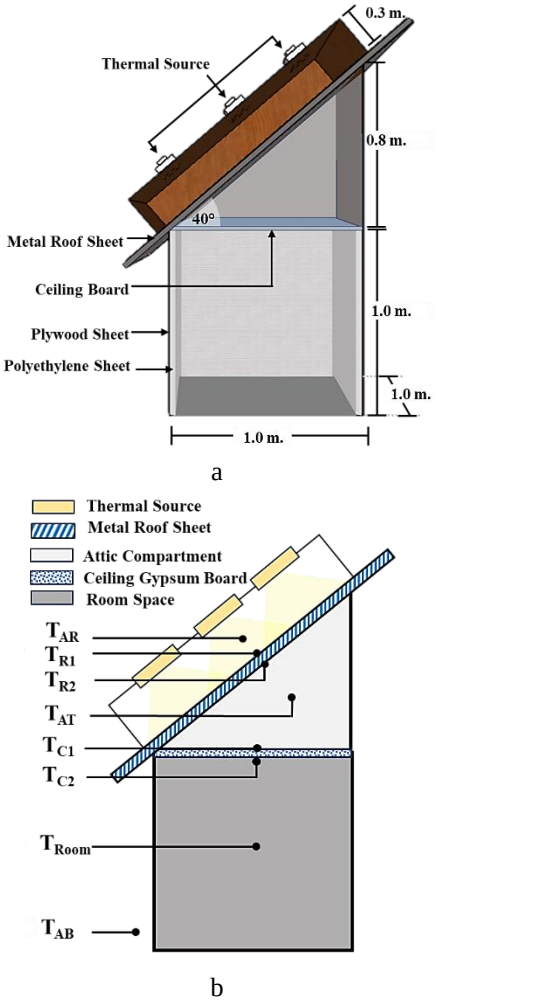

Fig. 4. Testing configuration: a – schematic representation of the testing model setup; b – configuration of fixed thermocouple positions in the model without the PCM layer

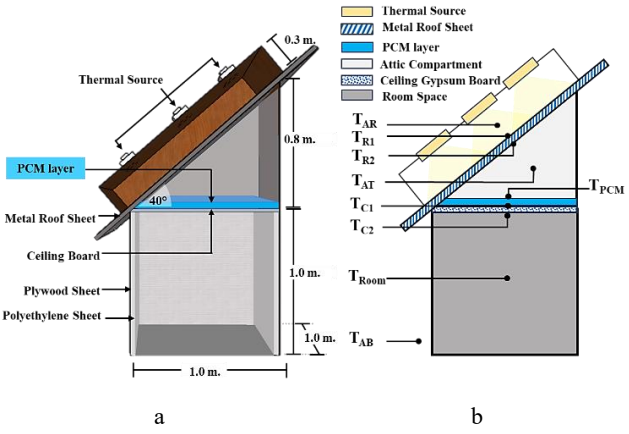

Fig. 5. Testing configuration: a – schematic representation of the testing model setup; b – configuration of fixed thermocouple positions in the model with a PCM layer on the ceiling

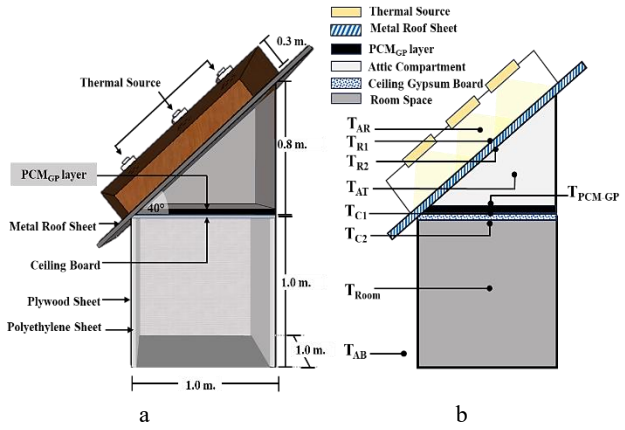

Fig. 6. Testing configuration: a – schematic representation of the testing pattern setup; b – design of the fixed thermocouple locations in the model with the PCM_{GP} layers (PCM_{GP} – 10 %, PCM_{GP} – 20 %) on the ceiling

3. RESULTS AND DISCUSSION

3.1. Thermal characteristics analysis of PCM and PCM_{GP}

The selection of a PCM for integrating into building frames to reduce cooling loads is an important decision in architectural and energy-efficient design. One of the key factors in this selection process is the phase change temperature range of the PCM [25]. For optimal performance and efficiency, it's important that the phase change temperature range of the PCM remains below the temperature level of the building envelope [26]. The main emphasis of this research is on the thermal characteristics of paraffin when used as a PCM within a temperature range of 0 °C to 80 °C, which were considered to investigate the melting and solidification revolution by using DSC analysis. The DSC analysis revealed two distinct curves of heat flow against temperature, representing endothermic and exothermic peaks (Fig. 7). Between 0 °C and 80 °C, the endothermic reaction curve displayed two negative peaks. The first endothermic peak (T_{En}) occurred around 43.4 °C with a heat (ΔH_{En}) of 36.38 J/g, signifying the initiation of the paraffin melting process. A subsequent endothermic peak (T_{EnL}) emerged at approximately 59.6 °C, exhibiting a latent heat (ΔH_{EnL}) of 155.83 J/g, signifying the continuous phase transition of paraffin into a liquid state from the initial peak. As the temperature decreased from 80°C to 0°C, the analysis revealed the presence of two separate exothermic reaction peaks. The first broad exothermic peak (T_{ExL}) at around 58.5 °C, with a latent heat (ΔH_{ExL}) of 148.04 J/g, and a secondary, smaller exothermic peak at approximately 40.4 °C (T_{Ex}). This exothermic peak showed with a heat of 23.91 J/g (ΔH_{Ex}), was related to the solidification process, and attributed to the thermal release of paraffin. This study is mainly concerned with the thermal properties of paraffin as a PCM, which were investigated using DSC analysis over a temperature range of 0 °C to 80 °C. The results of the study emphasized the beneficial range of melting and solidification temperatures exhibited by this particular paraffin-based PCM. This specific temperature range makes it particularly well-suited for applications focused on reducing interior temperatures within buildings and enhancing overall energy efficiency and comfort levels within structures. This is particularly relevant in tropical regions where roof temperatures, particularly metal roofs, can reach around 70 °C or higher during warm days [27].

The study investigated the various mass ratios of GP affect the phase change characteristics of PCM-based composites. Two distinct mixtures were created, comprising 10 % and 20 % GP by mass. The thermal properties of these composites, along with the pure PCM, were evaluated using DSC in a temperature range of 0 °C to 80 °C as exhibited in Fig. 7 and Table 1. With the incorporation of GP, the DSC result of the composites closely resembled those of the pure PCM. However, minor shifts were observed in the melting and solidification points. The initial PCM showed a melting point of 59.6 °C. Incorporating 10 % and 20 % GP led to marginal increases in the melting point, measuring 59.6 °C and 59.8 °C, respectively. For the solidification of the pure PCM, the point was at 58.3 °C. With 10 % and 20 % GP, slight reductions in solidification temperatures were noted, at 57.5 °C and 56.8 °C, respectively. Additionally, the DSC curves of the PCM-GP composites closely resembled those of the pure PCM. This similarity implies that the incorporation of GP did not lead to chemical alterations or change the intrinsic chemical properties of the PCM [28].

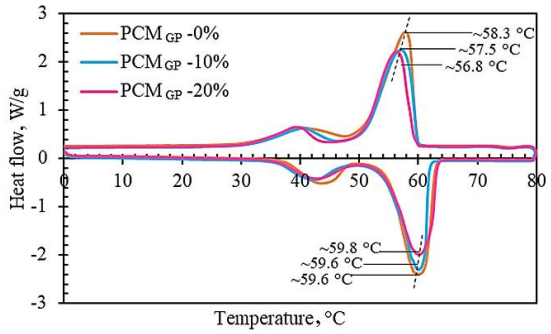

Fig. 7. DSC results illustrating the thermal characteristics of the PCM without infused GP (0 % GP), the PCM_{GP} – 10 %, and the PCM_{GP} – 20 % composites

The melting temperature range (T_{EnL}) widths for PCM (0 % GP), PCM_{GP} – 10 %, and PCM_{GP} – 20 % composites were approximately 8.5 °C, 6.3 °C, and 8.1 °C, respectively. Conversely, when examining the solidification temperature range (T_{ExL}) for these materials, they exhibited widths of approximately 8.9 °C, 8.5 °C, and 8.8 °C, as illustrated in Table 1.

Table 1. Thermal characteristics from DSC results of the PCM without incorporated GP (0 % GP), the PCM_{GP} – 10 %, and the PCM_{GP} – 20 % composites

Reaction of heat	Thermal characteristics		Conditions		
			PCM	PCM_{GP}-10%	PCM_{GP}-20%
Endothermic 0°C →80°C	T_{En}	°C	43.4	42.5	42.1
	ΔH_{En}	J/g	36.38	29.89	28.24
	T_{EnL}	°C	59.6	59.6	59.8
	ΔH_{EnL}	J/g	155.83	138.09	128.24
	W_{EnL}	°C	8.5	6.3	8.1
Exothermic 80°C →0°C	T_{Ex}	°C	40.4	40.4	39.3
	ΔH_{Ex}	J/g	23.91	27.09	27.29
	T_{ExL}	°C	58.3	57.5	56.8
	ΔH_{ExL}	J/g	148.04	138.70	129.42
	W_{ExL}	°C	8.9	8.5	8.8

The $PCM_{GP}-10\ \%$ composite exhibited a narrower temperature range of phase change process compared to both the PCM without GP (0 % GP) and $PCM_{GP}-20\ \%$ composite configurations. This reduction indicates the usefulness of GP in enhancing the thermal performance of paraffin. In particular, during the endothermic process, $PCM_{GP}-10\ \%$ exhibits a 25.88 % reduction in melting time compared to PCM (0 % GP). This improvement surpasses the 16.6 % thermal efficiency enhancement achieved by PCM (stearic acid) with nano-Al_2O_3 additives [17] and approaches the 29.54 % reduction obtained by incorporating 95 % porous copper metal foam into the PCM storage system [20]. The study highlights the improvement achieved through the $PCM_{GP}-10\ \%$ composite, emphasizing its potential to enhance thermal properties through the incorporation of GP, known for its high thermal conductivity, into PCM. This addition facilitates more uniform and rapid heat distribution, thereby enhancing the efficiency of heat exchange between PCM and the environment. Consequently, PCM transitions into the heat storage and release phases more effectively, resulting in only minor changes in the melting and solidification temperature points without affecting the temperature range and unique phase transition characteristics of PCM. The findings emphasize the feasibility of optimizing the proportion of GP in the composite to achieve the desired thermal characteristics, thereby contributing to the advancement of PCM-based materials in various thermal management applications.

3.2. Thermal behavior of different testing conditions

3.2.1. Average temperatures at various locations for each condition

When the thermal source was kept at a constant temperature of 60 °C, the variations in T_{AR}, T_{R1}, T_{R2}, T_{AT}, T_{PCM}, T_{C1}, T_{C2}, and T_{AB} were monitored for cases involving no PCM layer, a PCM layer without GP, a $PCM_{GP}-10\ \%$ layer, and a $PCM_{GP}-20\%$ layer, as shown in Fig. 8. The ambient temperature was maintained at approximately 25 °C. The temperature at each position was recorded every minute for 300 minutes. For the no-PCM layer condition (Fig. 8 a), the temperature at each position progressively increases from the ambient temperature and begins to stabilize at all positions after 90 minutes. The temperature stability at each position is contingent on the distance from the heat source, leading to variations in heat transmission. The average temperatures at T_{AR}, T_{R2}, T_{AT}, T_{C1}, T_{C2}, and T_{AB} positions were approximately 51.3 °C, 51.8 °C, 32.3 °C, 31.8 °C, 32.0 °C, and 25.1 °C, respectively, as shown in Table 2. The temperature variations in each location for the PCM layer (0 % GP), $PCM_{GP}-10\ \%$ layer, and $PCM_{GP}-20\ \%$ layer on the ceiling board at a fixed temperature of 60 °C were similar to those of the no-PCM layer model, as depicted in Fig. 8 b–d. Average temperatures at each location in all patterns increased as the temperature was raised from 60 °C to 70 °C and 80 °C, as outlined in Table 2. This indicates that the temperature variations observed in controlled testing may differ from those in real weather conditions, which can fluctuate with daily weather patterns [29].

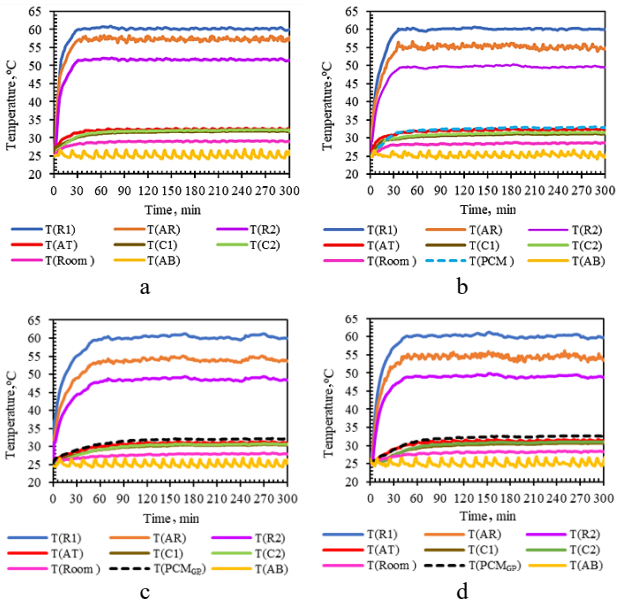

Fig. 8. Temperature evolution across different locations at a consistent temperature of 60°C: a – No-PCM layer; b – PCM layer (0 % GP); c – $PCM_{GP}-10\ \%$ layer; d – $PCM_{GP}-20\ \%$ layer on ceiling board

Table 2. Average temperatures at each position under different conditions of controlled temperature (60 °C, 70 °C and 80 °C)

$T_{controlled}$	Conditions	Average temperature at each location, °C							
		T_{R1}	T_{AR}	T_{R2}	T_{AT}	T_{PCM}	T_{C1}	T_{C2}	T_{AB}
60 °C	Without PCM	60.2	51.3	51.8	32.3	–	31.8	32.0	25.1
	PCM	60.1	52.0	49.7	31.8	32.8	30.7	31.0	25.2
	$PCM_{GP}-10\ \%$	60.2	53.9	48.6	30.9	32.0	30.2	30.5	25.2
	$PCM_{GP}-20\ \%$	60.0	54.5	49.1	31.4	32.5	30.5	30.8	25.2
70 °C	Without PCM	70.1	66.5	59.2	34.4	–	33.6	35.2	25.1
	PCM	70.0	63.1	56.6	33.9	34.7	32.9	33.3	25.2
	$PCM_{GP}-10\ \%$	70.2	61.9	55.8	33.2	34.2	31.0	32.1	25.1
	$PCM_{GP}-20\ \%$	70.1	62.4	56.2	33.6	34.5	32.2	32.8	25.2
80 °C	Without PCM	80.0	75.2	66.2	36.2	–	34.9	36.7	25.1
	PCM	80.1	72.5	64.9	35.3	36.2	33.4	34.2	25.1
	$PCM_{GP}-10\ \%$	80.1	70.2	62.8	34.2	35.0	32.9	33.1	25.2
	$PCM_{GP}-20\ \%$	80.1	71.4	63.5	34.9	35.4	33.0	33.8	25.1

In addition, the paraffin PCM examined demonstrates an indefinite number of heat emission cycles and does not rot, thereby averting material degradation over time. Its installation is analogous to that of general thermal insulation sheets, thereby maintaining the integrity of the original building structure. Furthermore, the selection of PCM based on DSC results allows for adaptation to diverse environments beyond controlled laboratory conditions. This study underscores the importance of the temperature range during the melting and solidification processes of PCM, along with ambient temperature, as critical factors influencing the efficiency of heat absorption and emission. Consequently, meticulous selection is imperative to ensure optimal performance under varying conditions

3.2.2. Decrement factor of each condition

The temperature differences (ΔT) between T_{R1} and T_{Room} under various controlled temperatures settings are displayed in Table 3, along with the temperature difference (ΔT) between the exterior surface and the interior of the testing room for each condition. With the thermal source consistently maintained at 60 °C, the temperature differences for the configuration without a PCM layer, with the PCM layer (0 % GP), $PCM_{GP}-10$ % layer, and $PCM_{GP}-20$ % layer installed on the ceiling board were approximately 31.2 °C, 31.6 °C, 32.3 °C, and 31.7 °C, respectively. In the absence of a PCM layer, ΔT surged from 31.2 °C to 49.2 °C as there was an increase of the controlled temperature from 60 °C to 80 °C that was controlled by using the thermal source. The temperature difference trends for conditions involving the PCM layer (0 % GP), $PCM_{GP}-10$ % layer, and $PCM_{GP}-20$ % layer installation on the ceiling board were similar to those of the pattern without installing a PCM layer, as outlined in Table 3.

Temperature decrement factors were assessed at both the outside roof surface and inner space in each model, and compared across different configurations: without a PCM layer, with PCM (0 % GP), $PCM_{GP}-10$ % layer, and $PCM_{GP}-20$ % layer at constant controlled temperatures of 50 °C, 60 °C, 70 °C, and 80 °C. These findings are detailed in Table 3 and Fig. 9 a. The temperature decrement factor (ʃ) is important as it indicates the percentage reduction in heat transfer through the outside roof surface into the inside testing model in each condition.

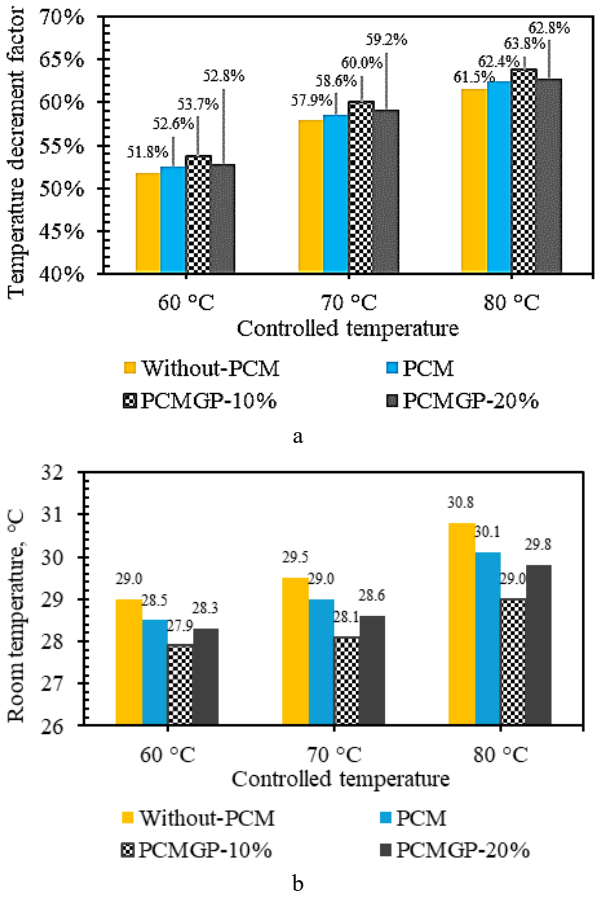

Fig. 9. The temperature decrement factor (ʃ) and average inside room temperatures of various models

The calculation of decrement factor is based on Eq. 2, emphasizing the importance of these factors in understanding how various configurations affect thermal transmission [33].

$$\text{Temperature decrement factor } (ʃ) = \frac{TR1 - TRoom}{TR1} \times 100\% = \frac{\Delta T}{TR1} \times 100\% . \quad (2)$$

In the absence of a PCM layer, the temperature decrement factor (ʃ) for the position of the outside roofing sheet surface (T_{R1}) to the position of the inside temperature of the model (T_{Room}) increased from 51.8 % to 61.5 % when the temperature at the outer roof surface increase from 60 °C to 80 °C.

Table 3. Average temperatures (T_{R1} and T_{Room}), temperature difference (ΔT), percentage of temperature decrement factor (ʃ), under different controlled temperature of each condition

$T_{controlled}$	Conditions	Average temperature, °C		ΔT	Temperature decrement factor (ʃ)
		T_{R1}	T_{Room}	(°C)	
60 °C	Without-PCM	60.2	29.0	31.2	51.8%
	PCM	60.1	28.5	31.6	52.6%
	PCM_{GP}-10%	60.2	27.9	32.3	53.7%
	PCM_{GP}-20%	60.0	28.3	31.7	52.8%
70 °C	Without-PCM	70.1	29.5	40.6	57.9%
	PCM	70.0	29.0	41.0	58.6%
	PCM_{GP}-10%	70.2	28.1	42.1	60.0%
	PCM_{GP}-20%	70.1	28.6	41.5	59.2%
80 °C	Without-PCM	80.0	30.8	49.2	61.5%
	PCM	80.1	30.1	50.0	62.4%
	PCM_{GP}-10%	80.1	29.0	51.1	63.8%
	PCM_{GP}-20%	80.1	29.8	50.3	62.8%

The tendency of decrement factor for the pattern with integrated PCM (0 % GP), $PCM_{GP}-10$ % layer, and $PCM_{GP}-20$ % layer conditions mirrored that of the configuration without a layer of PCM, as exhibited in Table 3 and Fig. 9 a. The integration of the PCM_{GP}-10% layer exhibited higher ΔT and higher temperature decrement factors, attributable to the heat absorption capabilities of the PCM, thereby exhibiting insulating properties. Moreover, the addition of GP in optimal proportions enhanced the heat absorption and emission performance of the PCM, effectively reducing heat transmission through the roof structure and mitigating heat accumulation within the house. This improvement significantly contributes to energy conservation in buildings [30, 31].

3.3. Comparison of average inside room temperatures

Table 3 and Fig. 9 b present the average indoor room temperature (T_{Room}) for each condition at various controlled temperatures. At a controlled temperature of 60 °C, the average T_{Room} values of the configuration without a PCM layer, with integrating PCM (0 % GP), $PCM_{GP}-10$ % layer, and $PCM_{GP}-20$ % layer conditions were approximately 29.0 °C, 28.5 °C, 27.9 °C, and 28.3 °C, respectively. The $PCM_{GP}-10$ % layer condition exhibited the lowest average T_{Room}, surpassing the other conditions by approximately 3.79 %, 2.11 %, and 1.41 %, respectively, compared to the configuration without a PCM layer, with integrated PCM layer (0 % GP), and $PCM_{GP}-20$ % layer conditions. In the absence of a PCM layer, the increase of average T_{Room} was at around 29.5 °C and 30.8 °C when the testing temperature was constantly controlled to 70 °C and 80 °C, respectively. The average T_{Room} for the other models also exhibited a similar upward trend as the model without a PCM layer (Fig. 9 b). Notably, the testing model with PCM and PCM_{GP} layers, particularly the $PCM_{GP}-10$ % layer, demonstrated a reduction in average T_{Room} in contrast to the setup without PCM integration across all controlled temperature conditions. The successful integration of GP-infused PCM into gypsum ceiling boards has demonstrated significant potential for improving indoor thermal comfort and reducing energy consumption. These findings suggest broader applications for GP-infused PCM in diverse building components, such as walls, roofs, and flooring. To fully realize the benefits of this technology, further research and development are required to optimize material performance, address economic viability, and ensure compliance with building regulations. Ultimately, widespread adoption of graphite-infused PCM in the construction industry could contribute substantially to the creation of more sustainable and energy-efficient buildings [32, 33].

Furthermore, the incorporation of PCM and PCM_{GP} into construction materials on a larger scale is possible, depending on the type of PCM. Paraffin, an organic PCM derived from petroleum products, is cheap, readily available, stable in absorbing and releasing heat, has an infinite cycle of usage, is water-insoluble, chemically inert, and is not harmful to packaging or building structures, and has no negative impact on the environment. However, paraffin has a low thermal conductivity, which can be improved by incorporating GP. GP is lightweight, cost-effective, and has a high thermal conductivity, making it the most suitable method compared to metal fins, metal powder particles, or graphene powder.

Additionally, this study on PCM encapsulation and analysis encounters several limitations, including:

1. Material and experimental constraints: Variations in paraffin source, small experimental scale, and limited temperature control conditions may not accurately reflect real-world performance.
2. Material properties and performance: Inconsistent graphite distribution, polyethylene encapsulation limitations, and the exclusive focus on paraffin restrict the evaluation of optimal material combinations and their long-term durability.
3. Environmental and economic considerations: The study neglects the environmental impact of materials and lacks economic analysis, hindering a comprehensive assessment of sustainability.
4. Research scope limitations: The study's focus on temperature measurements limits insights into heat transfer mechanisms. Additionally, the absence of comparisons with real-world data and safety evaluations restricts practical applications.

Addressing these limitations is essential for progressing the application of PCMs in sustainable building design.

4. CONCLUSIONS

Incorporating graphite-infused PCM into gypsum ceiling boards for building envelope applications has the potential to diminish heat propagation through the building envelope. The gypsum ceiling boards with integrated PCM and PCM infused with graphite ($PCM_{GP}-10$ %, $PCM_{GP}-20$ %) exhibited lower room temperatures, resulting in a reduction of the average room temperature by up to 1.72 %, 3.79 %, and 2.41 %, respectively, when the outside roof surface temperature was set at 60 °C. In comparison to these results models without a PCM layer underscores the effectiveness of incorporating PCM and graphite-infused PCM in enhancing thermal performance. Furthermore, the model incorporating the $PCM_{GP}-10$ % layer demonstrated an increased temperature decrement factor of approximately 3.67 %, 3.63 %, and 3.74 % at controlled temperatures of 60 °C, 70 °C, and 80 °C, respectively, compared to the model without a PCM layer. This suggests that integrating PCM and graphite-infused PCM into gypsum ceiling boards results in a more substantial reduction in room temperatures and a stronger temperature gradient, thereby improving the ceiling's insulating materials within the roof structure. This enhancement has the potential to decrease energy consumption from air conditioner cooling loads and decrease the annual peak cooling demand. Furthermore, PCM_{GP} composites have been developed as a highly effective way for sustainable building design. Integrating these materials into building envelopes contributes to a more sustainable future by reducing energy consumption and enhancing thermal performance, potentially leading to more energy-efficient and sustainable buildings.

Acknowledgements

The authors gratefully acknowledge the Science Achievement Scholarship of Thailand (SAST) and the Faculty of Science, Naresuan University, for their invaluable contributions to this research. This research was supported by the Thailand Science Research and Innovation (TSRI) through the Fundamental Fund (2023), under grant number R2566B015.

REFERENCES

1. **Cao, X., Dai, X., Liu, J.** Building Energy-consumption Status Worldwide and the State-of-the-art Technologies for Zero-energy Buildings During the Past Decade *Energy and Buildings* 128 2016: pp. 198 – 213. https://doi.org/10.1016/j.enbuild.2016.06.089
2. **Aydin, Y.C., Mirzaei, P.A., Akhavannasab, S.** On the Relationship between Building Energy Efficiency, Aesthetic Features and Marketability: Toward a Novel Policy for Energy Demand Reduction *Energy Policy* 128 2019: pp. 593 – 606. https://doi.org/10.1016/j.enpol.2018.12.036
3. **Lundgren, K., Kjellstrom, T.** Sustainability Challenges from Climate Change and Air Conditioning Use in Urban Areas *Sustainability* 5(7) 2023: pp. 3116 – 3128. https://doi.org/10.3390/su5073116
4. **Gou, Z., Gamage, W., Lau, S.S.Y., Lau, S.S.Y.** An Investigation of Thermal Comfort and Adaptive Behaviors in Naturally Ventilated Residential Buildings in Tropical Climates: A Pilot Study *Buildings* 8 (1) 2018: pp. 5. https://doi.org/10.3390/buildings8010005
5. **Bhamare, D.K., Rathod, M.K., Banerjee, J.** Passive Cooling Techniques for Building and Their Applicability in Different Climatic Zones – The State of Art *Energy and Buildings* 198 2019: pp. 467 – 490. https://doi.org/10.1016/j.enbuild.2019.06.023
6. **Khademi, A., Shank, K., Mehrjardi, S.A.A., Tiari, S., Sorrentino, G., Said, Z., Chamkha, A.J., Ushak, S.** A Brief Review on Different Hybrid Methods of Enhancement within Latent Heat Storage Systems *Journal of Energy Storage* 54 2022: pp. 105362. https://doi.org/10.1016/j.est.2022.105362
7. **Oh, J., Wong, W., Castro-Lacouture, D., Lee, J., Koo, C.** Indoor Environmental Quality Improvement in Green Building: Occupant Perception and Behavioral Impact *Journal of Building Engineering* 69 2023: pp. 106314. https://doi.org/10.1016/j.jobe.2023.106314
8. **Khademi, A., Mehrjardi, S.A.A., Said, Z., Saidur, R., Ushak, S., Chamkha, A.J.** A Comparative Study of Melting Behavior of Phase Change Material with Direct Fluid Contact and Container Inclination *Energy Nexus* 10 2023: pp. 100196. https://doi.org/10.1016/j.nexus.2023.100196
9. **Mehrjardi, S.A.A., Khademi, A., Said, Z., Ushak, S., Chamkha, A.J.** Enhancing Latent Heat Storage Systems: The Impact of PCM Volumetric Ratios on Energy Storage Rates with Auxiliary Fluid Assistance *Energy Nexus* 11 2023: pp. 100227. https://doi.org/10.1016/j.nexus.2023.100227
10. **Khan, R.J., Bhuiyan, M.Z.H., Ahmed, D.H.** Investigation of Heat Transfer of a Building Wall in the Presence of Phase Change Material (PCM) *Energy and Built Environment* 1 (2) 2020: pp. 199 – 206. https://doi.org/10.1016/j.enbenv.2020.01.002
11. **Li, S., Zhou, Y., Zhong, K., Zhang, X., Jin, X.** Thermal Analysis of PCM-filled Glass Windows in Hot Summer and Cold Winter Area *International Journal of Low-Carbon Technologies* 11 (2) 2016: pp. 275 – 282. https://doi.org/10.1093/ijlct/ctt073
12. **Kitagawa, H., Asawa, T., Kubota, T., Trihamdani, A.R.** Numerical Simulation of Radiant Floor Cooling Systems using PCM for Naturally Ventilated Buildings in a Hot and Humid Climate *Building and Environment* 226 2022: pp. 109762. https://doi.org/10.1016/j.buildenv.2022.109762
13. **Chung, M.H., Park, J.C.** Development of PCM Cool Roof System to Control Urban Heat Island Considering Temperate Climatic Conditions *Energy and Buildings* 116 2016: pp. 341–348. https://doi.org/10.1016/j.enbuild.2015.12.056
14. **Yang, S., Zhang, Y., Zhao, Y., Torres, J.F., Wang, X.** PCM-based Ceiling Panels for Passive Cooling in Buildings: A CFD Modelling *Energy and Buildings* 285 2023: pp. 112898. https://doi.org/10.1016/j.enbuild.2023.112898
15. **Paul, J., Samykano, M., Pandey, A.K., Kadirgama, K., Tyagi, V.V.** Nano Engineered Paraffin-Based Phase Change Material for Building Thermal Management *Buildings* 13 (4) 2023: pp. 900. https://doi.org/10.3390/buildings13040900
16. **Khademi, A., Mehrjardi, S.A.A., Said, Z., Chamkha, A.J.** Heat Transfer Improvement in a Thermal Energy Storage System using Auxiliary Fluid Instead of Nano-PCM in an Inclined Enclosure: A Comparative Study *Journal of Applied and Computational Mechanics* 9 (2) 2023: pp. 475 – 486. https://doi.org/10.22055/JACM.2022.41867.3829
17. **Yadav, C., Sahoo, R.R.** Effect of Nano-enhanced PCM on the Thermal Performance of a Designed Cylindrical Thermal Energy Storage System *A Journal of Thermal Energy Generation, Transport, Storage, and Conversion* 34 (4) 2022: pp. 356 – 375. https://doi.org/10.1080/08916152.2020.1751744
18. **Borhani, S.M., Hosseini, M.J., Pakrouh, R., Ranjbar, A.A., Nourian, A.** Performance Enhancement of a Thermoelectric Harvester with a PCM/Metal Foam Composite *Renewable Energy* 168 2021: pp. 1122 – 1140. https://doi.org/10.1016/j.renene.2021.01.020
19. **Kim, H.G., Qudoos, A., Jeon, I.K., Woo, B.H., Ryou, J.S.** Assessment of PCM/SiC-based Composite Aggregate in Concrete: Energy Storage Performance *Construction and Building Materials* 258 2020: pp. 119637. https://doi.org/10.1016/j.conbuildmat.2020.119637
20. **Falcone, M., Rehman, D., Dongellini, M., Naldi, C., Pulvirenti, B., Morini, G.L.** Experimental Investigation on Latent Thermal Energy Storages (LTESs) Based on Pure and Copper – Foam – Loaded PCMs *Energies* 15 (13) 2022: pp. 4894. https://doi.org/10.3390/en15134894
21. **Suyitno, B.M., Rahmalina, D., Rahman, R.A.** Increasing the Charge/discharge Rate for Phase Change Materials by Forming Hybrid Composite Paraffin/ash for an Effective Thermal Energy Storage System *AIMS Materials Science* 10 (1) 2023: pp. 70 – 85. https://doi.org/10.3934/matersci.2023005
22. **Oya, T., Nomura, T., Tsubota, M., Okinaka, N., Akiyama, T.** Thermal Conductivity Enhancement of Erythritol as PCM by using Graphite and Nickel Particles *Applied Thermal Engineering* 61 (2) 2013: pp. 825 – 828.

https://doi.org/10.1016/j.applthermaleng.2012.05.033

23. **Zhang, P., Cui, Y., Zhang, K., Wu, S., Chen, D., Gao, Y.** Enhanced Thermal Storage Capacity of Paraffin/diatomite Composite using Oleophobic Modification *Journal of Cleaner Production* 279 2021: pp. 123211. https://doi.org/10.1016/j.jclepro.2020.123211
24. **Magendran, S.S., Khan, F.S.A., Mubarak, N.M., Vaka, M., Walvekar, R., Khalid, M., Karri, R.R.** Synthesis of Organic Phase Change Materials (PCM) for Energy Storage Applications: A Review *Nano-Structures & Nano-Objects* 20 2019: pp. 100399. https://doi.org/10.1016/j.nanoso.2019.100399
25. **Masood, U., Haggag, M., Hassan, A., Laghari, M.** A Review of Phase Change Materials as a Heat Storage Medium for Cooling Applications in the Built Environment *Buildings* 13 (7) 2023: pp. 1595. https://doi.org/10.3390/buildings13071595
26. **Imafidon, O.J., Ting, D.S.K.** Energy Consumption of a Building with Phase Change Material Walls – The Effect of Phase Change Material Properties *Journal of Energy Storage* 52(Part C) 2022: pp. 105080. https://doi.org/10.1016/j.est.2022.105080
27. **Mano, C., Thongtha, A.** Enhanced Thermal Performance of Roofing Materials by Integrating Phase Change Materials to Reduce Energy Consumption in Buildings *Journal of Renewable Materials* 9 (3) 2021: pp. 495 – 506. https://doi.org/10.32604/jrm.2021.013201
28. **Feng, L., Wu, J., Sun, W., Cai, W.** Effects of Pore Structure and Pore Size of Expanded Graphite on the Properties of Paraffin Wax/Expanded Graphite Composite Phase Change Materials *Energies* 15 (12) 2022: pp. 4201. https://doi.org/10.3390/en15124201
29. **Mano, C., Thongtha, A., Maneewan, S., Punlek, C.** Improvement of the Thermal Efficiency of Autoclaved Aerated Concrete by Black Powder *ScienceAsia* 47S 2021: pp. 76 – 82. https://doi.org/10.2306/scienceasia1513-1874.2021.S015
30. **Elawady, N., Bekheit, M., Sultan, A.A., Radwan, A.** Energy Assessment of a Roof-integrated Phase Change Materials, Long-term Numerical Analysis with Experimental Validation *Applied Thermal Engineering* 202 2022: pp. 117773. https://doi.org/10.1016/j.applthermaleng.2021.117773
31. **Chou, H.M., Chen, C.R., Nguyen, V.L.** A New Design of Metal-sheet Cool Roof using PCM *Energy and Buildings* 57 2013: pp. 42 – 50. https://doi.org/10.1016/j.enbuild.2012.10.030
32. **Dabaieh, M., Wanas, O., Hegazy, M.A., Johansson, E.** Reducing Cooling Demands in a Hot Dry Climate: A Simulation Study for Non-insulated Passive Cool Roof Thermal Performance in Residential Buildings *Energy and Buildings* 89 2015: pp. 142 – 152. https://doi.org/10.1016/j.enbuild.2014.12.034
33. **Punlek, C., Maneewan, S., & Thongtha, A.** Phase Change Material Coating on Autoclaved Aerated Lightweight Concrete for Cooling Load Reduction *Materials Science (Medžiagotyra)* 23(2) 2017: pp. 161 – 165. https://doi.org/10.5755/j01.ms.23.2.15451